Title

Unprecedented Fluorophore Photostability Enabled by Low-Loss Organic Hyperbolic Materials

Journal

Advanced Materials, 33(9)

ISSN

0935-9648

Authors

Lee, Yeon Ui
Li, Shilong
Bopp, Steven Edward
et al.

Publication Date

2021-03-01

DOI

10.1002/adma.202006496

Peer reviewed

HHS Public Access

Author manuscript

Adv Mater. Author manuscript; available in PMC 2022 January 22.

Published in final edited form as:

Adv Mater. 2021 March ; 33(9): e2006496. doi:10.1002/adma.202006496.

Unprecedented fluorophore photostability enabled by low loss organic hyperbolic materials

Yeon Ui Lee,
Department of Electrical and Computer Engineering, University of California, San Diego, 9500 Gilman Drive, La Jolla, California 92093, USA

Shilong Li,
Department of Electrical and Computer Engineering, University of California, San Diego, 9500 Gilman Drive, La Jolla, California 92093, USA

Steven Edward Bopp,
Materials Science and Engineering, University of California, San Diego, 9500 Gilman Drive, La Jolla, California 92093, USA

Junxiang Zhao,
Department of Electrical and Computer Engineering, University of California, San Diego, 9500 Gilman Drive, La Jolla, California 92093, USA

Zhaoyu Nie,
Department of Mechanical Engineering, University of California, Berkeley, California 94720, USA

Clara Posner,
Department of Pharmacology, University of California, San Diego, 9500 Gilman Drive, La Jolla, California 92093, USA

Sui Yang,
Department of Mechanical Engineering, University of California, Berkeley, California 94720, USA

Xiang Zhang,
Department of Mechanical Engineering, University of California, Berkeley, California 94720, USA

Jin Zhang,
Department of Pharmacology, University of California, San Diego, 9500 Gilman Drive, La Jolla, California 92093, USA

Zhaowei Liu
Department of Electrical and Computer Engineering, University of California, San Diego, 9500 Gilman Drive, La Jolla, California 92093, USA

Materials Science and Engineering, University of California, San Diego, 9500 Gilman Drive, La Jolla, California 92093, USA

zhaowei@ucsd.edu .

Supporting Information
Supporting Information is available from the Wiley Online Library or from the author.

Abstract

The dynamics of photons in fluorescent molecules plays a key role in fluorescence imaging, optical sensing, organic photovoltaics, and displays. Photobleaching is an irreversible photodegradation process of fluorophores, representing a fundamental limitation in relevant optical applications. Chemical reagents have been used to suppress the photobleaching rate but with exceptionally high specificity for each type of fluorophore. Here, using organic hyperbolic materials (OHMs), we demonstrate an optical platform to achieve unprecedented fluorophore photostability without any chemical specificity. A more than 500-fold lengthening of the photobleaching lifetime and a 230-fold increase in the total emitted photon counts were observed simultaneously. These exceptional improvements solely come from the low loss hyperbolic dispersion of OHM films and the large resultant Purcell effect in the visible spectral range. The demonstrated OHM platform may open up a new paradigm in nanophotonics and organic plasmonics for super-resolution imaging and the engineering of light-matter interactions at nanoscale.

Graphical Abstract

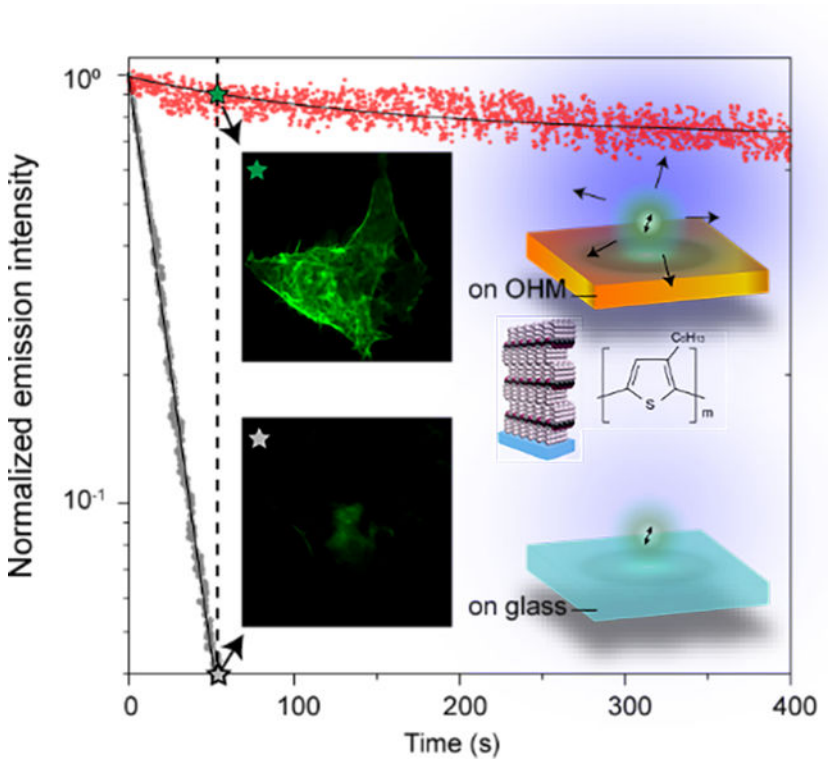

Fluorophores are much more photostable on OHMs than on glass. On the glass substrate, fluorophores are photobleached almost immediately; highly photostable fluorophores, however, are observed on the OHM substrate. Fluorophore photobleaching lifetimes were lengthened up to four orders of magnitude with a 230-fold increase in photon counts.

Keywords

photostability; organic hyperbolic materials; poly(3-hexylthiophenes); purcell effect; natural hyperbolic materials

Fluorescence microscopy[1] has been employed extensively to unveil sophisticated properties of specimens that cannot be seen with traditional microscopes and has thereby become an indispensable tool in numerous important applications in medicine[1], environmental studies[2], food sanitation[3], biological research[4], and industry[5]. However, these fluorescence-based sensing and imaging methods suffer from irreversible photobleaching[6] of fluorophores (i.e. a loss of their ability to fluoresce due to the photon-induced damage), which restricts the total number of emitted photons from each fluorophore. This photodegradation process eventually limits the maximum signal-to-noise ratio (SNR) and thus the sensitivity of a sensor[2,5] or the resolution of an image[7,8]. Therefore, it is crucial to enhance the fluorophore's photostability in order to improve the overall performance of fluorophore-based sensing and imaging systems.

Enormous efforts have been devoted to the enhancement of fluorophore photostability by varying either chemical or optical environments. The former method includes the introduction of chemical reagents[9]. However, these chemical reagents have to be carefully selected in order to avoid unintentional reactions or interactions with the specimens to be imaged. In another aspect, when the optical environment is modified, for example, by using plasmonic nanostructures[10–13], the photobleaching of a fluorophore is suppressed due to an enhancement of its spontaneous emission process. This phenomenon is known as Purcell effect and is caused by the enhanced photonic local density of states (LDOS) near the corners of the plasmonic nanostructures. Nevertheless, the high spatial locality of LDOS contributed by the plasmonic nanostructures not only introduces an additional complexity associated with nanofabrication but also substantially limits their potential applications where the performance of any locations on an interested plane cannot be sacrificed, e.g. wide-field imaging and sensing.

In a different context, hyperbolic materials[14,15] (i.e. the optical materials with a hyperbolic dispersion) have been the subject of extensive investigation over the past decade for their large potential in broad applications such as super-resolution imaging[16,17], refractive index sensing[18], engineering of optical nonlinearities[19], and enhancement of spontaneous emission[20,21]. It has been demonstrated that hyperbolic polariton modes supported by the hyperbolic materials lead to a strong and broadband Purcell effect even in their planar form[22–26]. Therefore, a layer of hyperbolic materials would be an ideal platform to improve the photostability of a fluorophore uniformly over the entire planar surface[27]. However, the nonradiative nature of these hyperbolic polariton modes and the inevitable material loss contributed from the metallic components of traditional hyperbolic metamaterials (HMMs) present major challenges in achieving a high photostability with a sufficient number of emitted photons.

In this letter, we demonstrate an unprecedented fluorophore photostability enabled by a self-assembled organic hyperbolic material (OHM) film[28] in the visible spectrum. Compared

to traditional HMMs[22,29,30] made of noble metal structures and other natural hyperbolic materials[31–33], the OHMs used in this work feature a Lorentz-type dispersion[33,34] with low-loss natural hyperbolic polariton modes[28], and thus support an extremely large LDOS and a large Purcell factor[35]. Moreover, this low-loss hyperbolic nature of the OHM films also makes an efficient fluorescence enhancement without any outcoupling structure possible. Therefore, it was observed that fluorophores near the OHMs showed a 230-fold increase in the total number of emitted photons, and a 500-fold prolonged photobleaching lifetime simultaneously. Such a remarkably enhanced fluorophore photostability may lead to various new opportunities where photobleaching is a concern.

An OHM of regioregular poly(3-hexylthiophene-2,5-diyl) (rr-P3HT) was self-assembled as described in Reference [[28]]. Figure S1a shows the complex permittivity of the fabricated rr-P3HT OHM film measured by variable angle spectroscopic ellipsometry (VASE). The film features low-loss hyperbolic behavior in the visible spectral range of 420–560 nm with the material figure of merit (FoM) $-\mathrm{Re}(\varepsilon_H)/\mathrm{Im}(\varepsilon_H) > 10$, where ε_H is the horizontal component of the complex permittivity[28] (see Supporting Information S2). With such a large FoM, the hyperbolic polariton modes supported by the OHM give rise to an exceptionally strong Purcell effect, originating from the excitations of the nonradiative high momentum (high-k) hyperbolic polariton modes (see Supporting Information S3) and the radiative modes (see Supporting Information S4 and S5). The low-loss hyperbolic nature of the OHMs also leads to a significant increase in the total emitted photon counts through the radiative leaky channel (see Supporting Information S5).

Figure 1a and 1b illustrate the basic underlying principle of the enhanced photostability of fluorophores by the hyperbolic modes of the OHM. A strong Purcell effect leads to an enhanced spontaneous emission decay rate ($PF = k_f/k_{f0}$, where k_f (k_{f0}) is a spontaneous emission decay rate of fluorophores on top of the OHM (glass).)[20–22], which subsequently reduces the probability of photochemical reactions of the fluorophores in the excited triplet state (T_1)[10–13] (see Supporting Information S6). Note that the Purcell factor (PF) is the sum of the radiative and nonradiative decay rate enhancements, i.e. $k_f/k_{f0} = k_r/k_{f0} + k_{nr}/k_{f0}$. The presence of the OHM also results in an electric field enhancement ($\Gamma_{exc} = I_{exc}/I_0$, where I_{exc} is an electric field intensity in the presence of the OHM.). Therefore, the total photobleaching rate $k_{pb,OHM}$ of fluorophores on top of the OHM can be described by $k_{pb,0} \times \Gamma_{exc}/PF$[11,27,36]. Note that the subscript 0 represents the corresponding quantities for fluorephores on glass substrate. Since Γ_{exc} with a plane wave is typically ~2 (see Supporting Information S7) while PF is on the order of a few hundreds to a few thousands (Figure 1c), the $k_{pb,OHM}$ of fluorophores is predominantly determined by the PF provided by the OHM. The enhancement of the total emitted photons (Figure 1d) is $S_{OHM}/S_0 = PF \times k_r/k_f = k_r/k_{f0}$[11], where S_{OHM} is the total emitted photons in the presence of the OHM. As can be clearly seen from Figures 1c and 1d, both the PF and S_{OHM}/S_0 are high, so that a strongly suppressed photobleaching of fluorophore (i.e. prolonged photobleaching lifetimes and increase in the total number of emitted photons) is expected with the OHM. Note that the PF can also be large when the fluorophore is placed close to a planar metallic surface: For example, the PF with a Ag film is about 10^2 at the wavelength $\lambda = 500$ nm. However, the corresponding radiative decay rate enhancement k_r/k_{f0} is only around 1.5 (see Supporting Information S4). Therefore, most of the emitted photons are converted to the

non-radiative modes and then dissipated in the metallic film. In contrast, in the case using the OHM, due to the excitation of the low-loss hyperbolic modes and the radiative coupling to the far field, there is a significant enhancement in the radiative component, i.e. k_r/k_{f0} reaches to 10^2; moreover, a higher k_r/k_{f0} is possible by considering roughened OHM films (see Supporting Information S4 and S5).

The photobleaching response of a fluorescent molecule refers to a degradation of the photon emission intensity over time; a photobleaching lifetime can be extracted from this response by mathematical fitting. Photobleaching experiments were carried out with a wide-field fluorescence microscope as shown in Figure 2a (see details in Methods). A 488-nm laser was used to excite molecules of fluorescein (Figure S1b) situated on top of the OHM films with an intensity of approximately 61 W/cm^2. Note that a nearly constant laser intensity was applied for all experiments to exclude any possible excitation-power dependence on the photobleaching dynamics. To study distance-dependent photobleaching dynamics caused by the distance-dependent *PF*, SiO_2 spacer layers with respective thicknesses d = 0, 5, 10, and 20 nm were sputtered onto four identical OHM films. A fluorescein/PVP layer with 2–5 nm thickness was spin-coated (see details in Methods) onto the top of the spacer layer. A band-pass filter (λ_{em} = 520/40 nm) was used to collect emission signals from the fluorescein molecules. 5000 frames of fluorescence images were collected with an exposure time of 200 ms at the imaging speed of 5 frames per second in order to obtain a complete photobleaching decay curve. To demonstrate enhanced photostability of fluorescein by the OHM in an intuitive way, the wide-field fluorescence images at various times throughout the exposure are shown in Figure 2b and 2c: On the glass substrates (Figure 2b), the fluorescein was completely destroyed after ~20 seconds; however, the emission degradation of the fluorescein on the OHM substrate occurred much more slowly (Figure 2c) and fluorescence was still visible after ~100 seconds.

A value for photobleaching lifetime can be extracted by fitting the photobleaching decay curve on a pixel by pixel basis. For the photobleaching curve of fluorescein on the control sample, a single-exponential decay function was used to obtain the photobleaching lifetime τ_0. For the OHM sample, a bi-exponential decay fitting was applied to the data, showing two photobleaching lifetimes: the first being relatively fast τ_1, and a second slower τ_2. This bi-exponential decay response can be interpreted as differences in the *PF*s arising from surface roughness of the OHM film and nonuniformity in dye layer thickness[37] (the dye layer contains both strongly- and weakly-interacting dye molecules on the OHM film). The quick photobleaching τ_1 is attributed to weakly-interacting dye molecules located above the coupling distance from the OHM (see details in Supporting Information S8).

The calculated distance-dependent *PF*s for the experimentally realized distances are given in Figure 3a and the calculated *PF*s at λ = 520 nm as a function of the distance to OHM surface are shown in Figure 3b. Figure 3c–3f give statistics of the photobleaching, obtained from the extracted photobleaching decay time from a 50×50 pixel (8.125×8.125 μm^2) area, showing a lengthening of photobleaching lifetime for fluorescein on an OHM substrate compared to that on a glass substrate. In Figure 3c, most of the dataset show a 200–1000× improvement, and some of the suppression factors reach a factor of 10^4×. Table 1 summarizes these average values, and averaged emission intensity decay curves are

given in Figure 3g. A significant modification of the fluorescein photobleaching dynamics resulting from the OHM is apparent. Strong dependence of photostability on distance from the OHM surface was observed; distance-dependent average photobleaching lifetimes are shown in Figure 3h–3i. Experimental results are in good agreement with the calculated *PF*s (see Figure 3b and Supporting Information S6–2).

Since the SNR is crucial for fluorescence microscopy, emission intensity I_t per frame and the total emission intensity $S = \sum I_t$ were investigated. In the beginning stage, fluorophores on glass substrate emit more photons than those on the OHM. For example, Figure 3j shows the normalized initial emission intensity $I_{0,\mathrm{OHM}}/I_{0,\mathrm{glass}}$ as a function of the distance between fluorophores and the OHM surface; these values are 0.55, 0.58, 0.60, and 0.64 for 0, 5, 10, and, 20 nm separations, respectively. This distance-dependent change in the normalized emission intensity is attributed to the introduction of a nonradiative decay channel due to the OHM material loss—in other words, a fraction of emitted photons will be absorbed by the OHM (see details in Supporting Information S7). Nevertheless, as demonstrated above, the photobleaching of fluorophores is much faster on glass than on the OHM (Figure 3g). As a result, above a certain time threshold, more photons are obtained from the OHM sample than the glass sample. Figure 3k shows the normalized total emission intensity $S_{\mathrm{OHM}}/S_{\mathrm{glass}}$ from fluorophores at different distances above the OHM surface; these values are 231, 75, 31, and 3 over the distance of 0, 5, 10, and 20 nm, respectively. This emission enhancement is attributed to the improvement of fluorescence photostability with the OHM since an increased emission time leads to more emitted photons and will give rise to a large SNR.

Fluorescence photostability improvements by the OHM were also clearly observed in bioimaging of a Lifeact-Venus tagged Cos-7 cell (Figure 4). In these cell images (Figure 4a–4d), the emission lifespan on the OHM surface exhibits a stronger photobleaching suppression compared to that of the control sample. Note that the distance of the Cos-7 cells with fluorescently labeled actin and plasma membrane from the substrate varies from 2 nm to 80 nm[27,38]. We believe that prolonged photobleaching lifetimes provide long-lasting fluorescence imaging for all fluorophores within the effective range of 0 to 60 nm (Figure 3b) along the axial direction.

A survey of experimentally obtained *PF*s in the visible spectrum among the most used HMMs and plasmonic materials, as well as the OHMs is shown in Figure S10. For a given plasmonic material, the Purcell effect originates from the surface plasmon resonance, and the maximum *PF* is obtained at the resonance peak wavelength. For Ag, the resonance peak wavelength is centered around 440 nm[39], and for Au it is centered at 620 nm[40–42]. TiN-based HMMs[43,44], Ag-based HMMs[20,21,23,33,45–50], and Au-based HMMs[40,51,52] support a broadband but relatively small *PF*. The OHMs used in this work provide *PF*s two orders of magnitude larger than the values found in those plasmonic materials, and even comparable to the values attained by using plasmonic nanostructures such as nanoantennae[11,41], nanocavities[53], and nanogratings[21,48] in the spectral range of 480–560 nm. Note that by exploiting the OHM's dispersion tunability[28], the *PF* and the corresponding operating wavelength can be further optimized.

In conclusion, we demonstrate a novel OHM platform with the record *PF*s at visible frequencies that significantly enhanced photostability of fluorophores. Fluorophore photobleaching lifetimes were lengthened up to four orders of magnitude with a 230-fold increase in photon counts (see a detailed comparison in Supporting Information S12). The performance can be further improved by, for example, optimizing the surface roughness and the thickness of OHM films. Such an OHM materials platform could enable a number of high-performance photonics applications such as organic photovoltaics, dye lasers, and fluorescence-based techniques including single-molecule tracking, biosensing, and various forms of super-resolution fluorescence microscopy. With its chemical tunability, fabrication simplicity, mechanical flexibility, and biocompatibility, the demonstrated OHM opens new avenues in nanophotonics.

Experimental Section

Samples for the variable angle spectroscopic ellipsometry (VASE) measurement:

To produce the OHM films, 100 mg of >98% regioregular head-to-tail P3HT molecules (Sigma Aldrich, average Mw ~ 87,000 g/mol) were dissolved in 1 ml of chlorobenzene (CB). These solutions were heated to 50 °C for 3 hours. The P3HT:CB solutions were spin-coated onto plasma-cleaned glass substrates. Film thicknesses of 182 nm were measured by both a DekTak surface profilometer and VASE. Here, VASE was also used to determine the permittivity spectra of the films. Please see the Supporting Information for details of VASE measurement.

Samples for the photobleaching experiment:

1 mg of fluorescein dye was dissolved in 1 mL of combined polyvinylpyrrolidone (PVP, Sigma-Aldrich, MW = 55000): ethanol solutions (0.01 wt %) to improve fluorophore uniformity in films. The coating solution was dispensed for each OHM film and spun for 5 s at 300 rpm and then 60 s at 5000 rpm. After spin coating, the fluorescein/PVP layer thickness (2~5 nm) was measured with VASE.

Experimental set-up:

We used an in-house modified fluorescence microscope (Olympus IX83). Upon excitation with a 488 nm laser (Coherent Genesis MX-488–1000 STM) coupled into a multimode fiber (Thorlabs, core diameter: 50 μm, NA 0.2), the substrate is illuminated with an intensity of approximately 61 W/cm^2. Constant laser intensity is applied for all the wide field illuminations in our experiments to exclude the excitation power dependence factor of photobleaching. The fluorescence signal is collected by an objective lens (80×/0.6 NA Olympus objective) and sent to an sCMOS camera (Hamamatsu ORCA_Flash4.0 V3 digital CMOS camera (C13440−20CU)) with proper emission filters. A 520/40 nm band-pass filter was used to remove the rr-P3HT emission contribution, and to collect the fluorescein emission. We acquired 5000 frames (5 frames per second) of emission signal and analyzed the resulting image stack using a mathematical fitting process with in-house developed code run in the MATLAB environment. To synchronize all equipment properly, we use MATLAB software to control a DAQ voltage output module (NI-9263) from National Instruments.

Finite-difference time-domain (FDTD) calculation:

The *PF* corresponds to an emission rate enhancement of a spontaneous emitter inside or near a cavity or plasmonic structure. Finite-difference time-domain (FDTD) simulations were performed using the Lumerical software to calculate the dispersion of the *PF*. By placing a dipole source on top of an OHM/glass substrate at $z = d$, the power emitted from the dipole in the presence of OHM/glass divided by the power emitted from the dipole in the absence of OHM/glass is calculated from 300 nm to 650 nm. The dipole emitter orientation in the dye layer was assumed to be random. The randomly oriented fluorophore is modeled by an average of 2/3 horizontal (H) dipoles and 1/3 of vertically (z) oriented dipoles. The experimentally obtained permittivity from ellipsometry measurements was used in the FDTD simulations. A minimum mesh step size of 0.25 nm is defined, and the perfectly matched layer's boundary conditions are adopted. The *PF* calculation includes both radiative and non-radiative decay rates associated with near-field coupling to the polaritonic resonance mode of the dipole located nearby the OHM. The dissipated power spectrum is calculated using a band structure simulation methodology. Bloch and PML boundary conditions and time monitors are used to calculate normalized dissipated power spectrum for the randomly oriented and randomly distributed dipoles near the OHM.

Sample preparation for Lifeact-Venus tagged Cos-7 cells:

Cos-7 cells were cultured in Dulbecco modified Eagle medium (DMEM; Gibco) containing 4.5 g/L glucose and supplemented with 10% (v/v) fetal bovine serum (FBS, Sigma) and 1% (v/v) penicillin-streptomycin (Pen-Strep, Sigma-Aldrich). Cells were maintained in a humidified incubator at 37°C with a 5% CO2 atmosphere. 24 hours prior to transfection, cells were seeded onto the glass or OHM substrates and grown to 50–70% confluence. Cells were then transfected with 100 ng of pcDNA3-Lifeact-Venus using Lipofectamine 2000 (Invitrogen) and grown an additional 24 h before imaging.

Supplementary Material

Refer to Web version on PubMed Central for supplementary material.

Acknowledgements

This work was supported by the Gordon and Betty Moore Foundation. Work at the Molecular Foundry was supported by the Office of Science, Office of Basic Energy Sciences, of the U.S. Department of Energy under Contract No. DE-AC02-05CH11231.

References

[1]. Lichtman JW, Conchello J-A, Nat. Methods 2005, 2, 910. [PubMed: 16299476]

[2]. Fischer T, Agarwal A, Hess H, Nat. Nanotechnol 2009, 4, 162. [PubMed: 19265845]

[3]. Preece KE, Drost E, Hooshyar N, Krijgsman A, Cox PW, Zuidam NJ, J. Food Eng 2015, 147, 8.

[4]. Betzig E, Patterson GH, Sougrat R, Lindwasser OW, Olenych S, Bonifacino JS, Davidson MW, Lippincott-Schwartz J, Hess HF, Science 2006, 313, 1642. [PubMed: 16902090]

[5]. Ameloot R, Vermoortele F, Hofkens J, De Schryver FC, De Vos D. E., Roeffaers MBJ, Angew. Chemie Int. Ed 2013, 52, 401.

[6]. Song L, Hennink EJJ, Young ITT, Tanke HJJ, Biophys. J 1995, 68, 2588. [PubMed: 7647262]

[7]. Dertinger T, Colyer R, Iyer G, Weiss S, Enderlein J, Proc. Natl. Acad. Sci 2009, 106, 22287. [PubMed: 20018714]

[8]. Shao L, Kner P, Rego EH, Gustafsson MGL, Nat. Methods 2011, 8, 1044. [PubMed: 22002026]

[9]. Rasnik I, McKinney SA, Ha T, Nat. Methods 2006, 3, 891. [PubMed: 17013382]

[10]. Munkhbat B, Wersäll M, Baranov DG, Antosiewicz TJ, Shegai T, Sci. Adv 2018, 4, eaas9552. [PubMed: 29984306]

[11]. Cang H, Liu Y, Wang Y, Yin X, Zhang X, Nano Lett. 2013, 13, 5949. [PubMed: 24245957]

[12]. Kaminska I, Vietz C, Cuartero-González Á, Tinnefeld P, Fernández-Domínguez AI, Acuna GP, Nanophotonics 2018, 7, 643.

[13]. Pellegrotti JV, Acuna GP, Puchkova A, Holzmeister P, Gietl A, Lalkens B, Stefani FD, Tinnefeld P, Nano Lett. 2014, 14, 2831. [PubMed: 24690008]

[14]. Poddubny A, Iorsh I, Belov P, Kivshar Y, Nat. Photonics 2013, 7, 948.

[15]. Ferrari L, Wu C, Lepage D, Zhang X, Liu Z, Prog. Quantum Electron 2015, 40, 1.

[16]. Liu Z, Lee H, Xiong Y, Sun C, Zhang X, Science 2007, 315, 1686. [PubMed: 17379801]

[17]. Sun J, Shalaev MI, Litchinitser NM, Nat. Commun 2015, 6, 7201. [PubMed: 25998241]

[18]. Vasilantonakis N, Wurtz GA, Podolskiy VA, Zayats AV, Opt. Express 2015, 23, 14329. [PubMed: 26072797]

[19]. Neira AD, Olivier N, Nasir ME, Dickson W, Wurtz GA, Zayats AV, Nat. Commun 2015, 6, 7757. [PubMed: 26195182]

[20]. Krishnamoorthy HNS, Jacob Z, Narimanov E, Kretzschmar I, Menon VM, Science 2012, 336, 205. [PubMed: 22499943]

[21]. Lu D, Kan JJ, Fullerton EE, Liu Z, Nat. Nanotechnol 2014, 9, 48. [PubMed: 24390565]

[22]. Jacob Z, Smolyaninov II, Narimanov EE, Appl. Phys. Lett 2012, 100, 181105.

[23]. Jacob Z, Kim J-Y, Naik GV, Boltasseva A, Narimanov EE, Shalaev VM, Appl. Phys. B 2010, 100, 215.

[24]. Noginov MA, Li H, Barnakov YA, Dryden D, Nataraj G, Zhu G, Bonner CE, Mayy M, Jacob Z, Narimanov EE, Opt. Lett 2010, 35, 1863. [PubMed: 20517443]

[25]. Newman WD, Cortes CL, Jacob Z, J. Opt. Soc. Am. B 2013, 30, 766.

[26]. Poddubny AN, Belov PA, Ginzburg P, Zayats AV, Kivshar YS, Phys. Rev. B 2012, 86, 1.

[27]. Lee YU, Zhao J, Mo GCH, Li S, Li G, Ma Q, Yang Q, Lal R, Zhang J, Liu Z, Nano Lett. 2020, 20, 6038. [PubMed: 32597659]

[28]. Lee YU, Yim K, Bopp SE, Zhao J, Liu Z, Adv. Mater 2020, 32, 2002387.

[29]. Zhukovsky SV, Kidwai O, Sipe JE, Opt. Express 2013, 21, 14982. [PubMed: 23787686]

[30]. Wood B, Pendry JB, Tsai DP, Phys. Rev. B 2006, 74, 115116.

[31]. Narimanov EE, Kildishev AV, Nat. Photonics 2015, 9, 214.

[32]. Gjerding MN, Pandey M, Thygesen KS, Nat. Commun 2017, 8, 1. [PubMed: 28232747]

[33]. Lee YU, Gaudin OPM, Lee K, Choi E, Placide V, Takaishi K, Muto T, André P, Muranaka A, Uchiyama M, Mathevet F, Aoyama T, Wu J, D'Aléo A, Ribierre J-C, ACS Photonics 2019, 6, 1681.

[34]. Lee YU, Garoni E, Kita H, Kamada K, Woo BH, Jun YC, Chae SM, Kim HJ, Lee KJ, Yoon S, Choi E, Mathevet F, Ozerov I, Ribierre JC, Wu JW, D'Aléo A, Adv. Opt. Mater 2018, 6, 1701400.

[35]. Li T, Khurgin JB, Optica 2016, 3, 1388.

[36]. Vasilev K, Stefani FD, Jacobsen V, Knoll W, Kreiter M, J. Chem. Phys 2004, 120, 6701. [PubMed: 15267562]

[37]. El Kabbash M., Rahimi Rashed A., Sreekanth KV, De Luca A, Infusino M, Strangi G, J. Nanomater 2016, 2016, 1.

[38]. Kanchanawong P, Shtengel G, Pasapera AM, Ramko EB, Davidson MW, Hess HF, Waterman CM, Nature 2010, 468, 580. [PubMed: 21107430]

[39]. Neogi A, Lee C-W, Everitt HO, Kuroda T, Tackeuchi A, Yablonovitch E, Phys. Rev. B 2002, 66, 153305.

[40]. Tsurumachi N, Izawa H, Tomioka R, Sakata T, Suzuki M, Tanaka Y, Shimokawa F, Nakanishi S, Jpn. J. Appl. Phys 2016, 55, 02BB05.

[41]. Hoang TB, Akselrod GM, Argyropoulos C, Huang J, Smith DR, Mikkelsen MH, Nat. Commun 2015, 6, 7788. [PubMed: 26212857]

[42]. Chizhik AI, Rother J, Gregor I, Janshoff A, Enderlein J, Nat. Photonics 2014, 8, 124.

[43]. Shalaginov MY, Vorobyov VV, Liu J, Ferrera M, Akimov AV, Lagutchev A, Smolyaninov AN, Klimov VV, Irudayaraj J, Kildishev AV, Boltasseva A, Shalaev VM, Laser Photon. Rev 2015, 9, 120.

[44]. Naik GV, Saha B, Liu J, Saber SM, Stach EA, Irudayaraj JMK, Sands TD, Shalaev VM, Boltasseva A, Proc. Natl. Acad. Sci 2014, 111, 7546. [PubMed: 24821762]

[45]. Lin HI, Shen KC, Liao YM, Li YH, Perumal P, Haider G, Cheng BH, Liao WC, Lin SY, Lin WJ, Lin TY, Chen YF, ACS Photonics 2018, 5, 718.

[46]. Lee KJ, Lee YU, Kim SJ, André P, Adv. Mater. Interfaces 2018, 5, 1701629.

[47]. Morozov KM, Ivanov KA, de Sa Pereira D, Menelaou C, Monkman AP, Pozina G, Kaliteevski MA, Sci. Rep 2019, 9, 9604. [PubMed: 31270385]

[48]. Lu D, Qian H, Wang K, Shen H, Wei F, Jiang Y, Fullerton EE, Yu PKL, Liu Z, Adv. Mater 2018, 30, 1.

[49]. Li L, Wang W, Luk TS, Yang X, Gao J, ACS Photonics 2017, 4, 501.

[50]. Shalaginov MY, Ishii S, Liu J, Liu J, Irudayaraj J, Lagutchev A, Kildishev AV, Shalaev VM, Appl. Phys. Lett 2013, 102, 173114.

[51]. Sreekanth KV, De Luca A, Strangi G, Sci. Rep 2013, 3, 1.

[52]. Lin H-I, Shen K, Lin S, Haider G, Li Y, Chang S, Chen Y, Sci. Rep 2018, 8, 9469. [PubMed: 29930247]

[53]. Sorger VJ, Pholchai N, Cubukcu E, Oulton RF, Kolchin P, Borschel C, Gnauck M, Ronning C, Zhang X, Nano Lett. 2011, 11, 4907. [PubMed: 21978206]

[54]. Kim J, Drachev VP, Jacob Z, Naik GV, Boltasseva A, Narimanov EE, Shalaev VM, Opt. Express 2012, 20, 8100. [PubMed: 22453481]

[55]. Creatore C, Andreani LC, Miritello M, Lo Savio R, Priolo F, Appl. Phys. Lett 2009, 94, 103112.

[56]. Vasilantonakis N, Nasir ME, Dickson W, Wurtz GA, Zayats AV, Laser Photon. Rev 2015, 9, 345. [PubMed: 26693254]

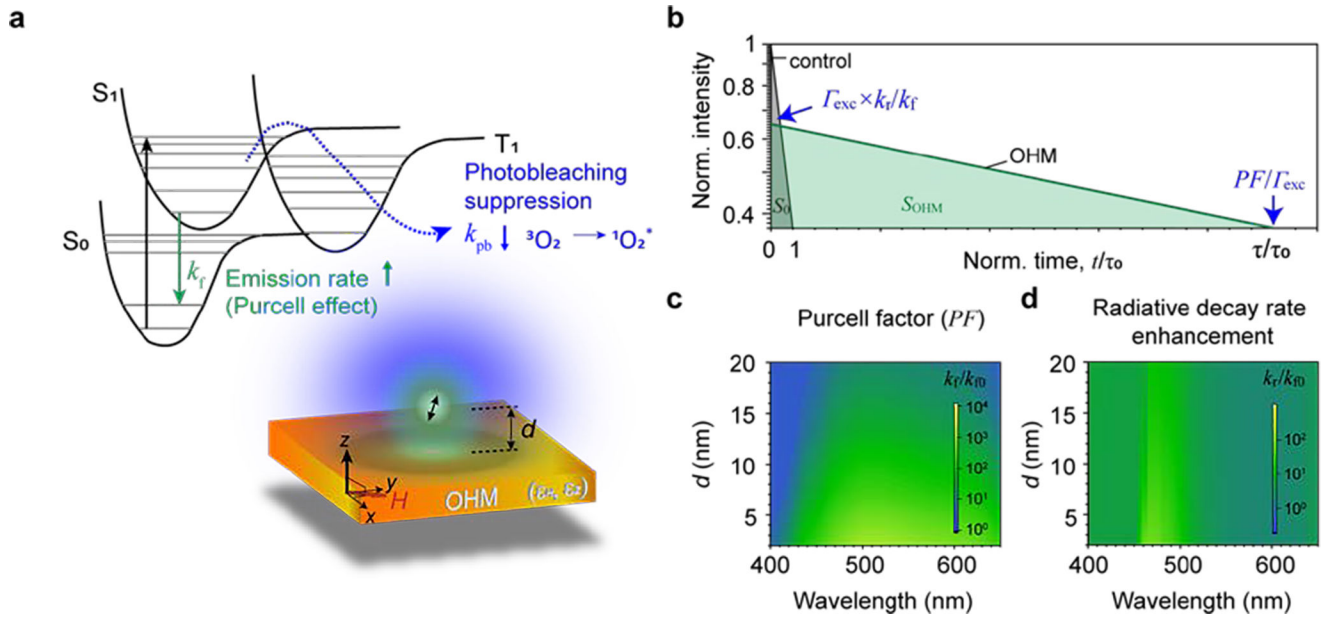

Figure 1.

Photobleaching suppression near OHMs. (**a**) Simplified schematic energy diagram and photostability enhancement by Purcell effect. The Purcell factor (*PF*) is a key quantity that describes the coupling rate between a dipole emitter and hyperbolic modes of a planar OHM (see the inset). Photobleaching rate k_{pb} of a fluorophore on top of the OHM is inversely proportional to the *PF*. (**b**) Schematic drawing of the fluorescence intensity over time for fluorophores on glass and on OHM. Wavelength and distance dependences of the *PF* (**c**) and the radiative decay rate enhancement (**d**). The *PF* comes from both the radiative k_r/k_{f0} and the nonradiative k_{nr}/k_{f0} components. The radiative decay rate enhancement represents the increase of the total number of emitted photons.

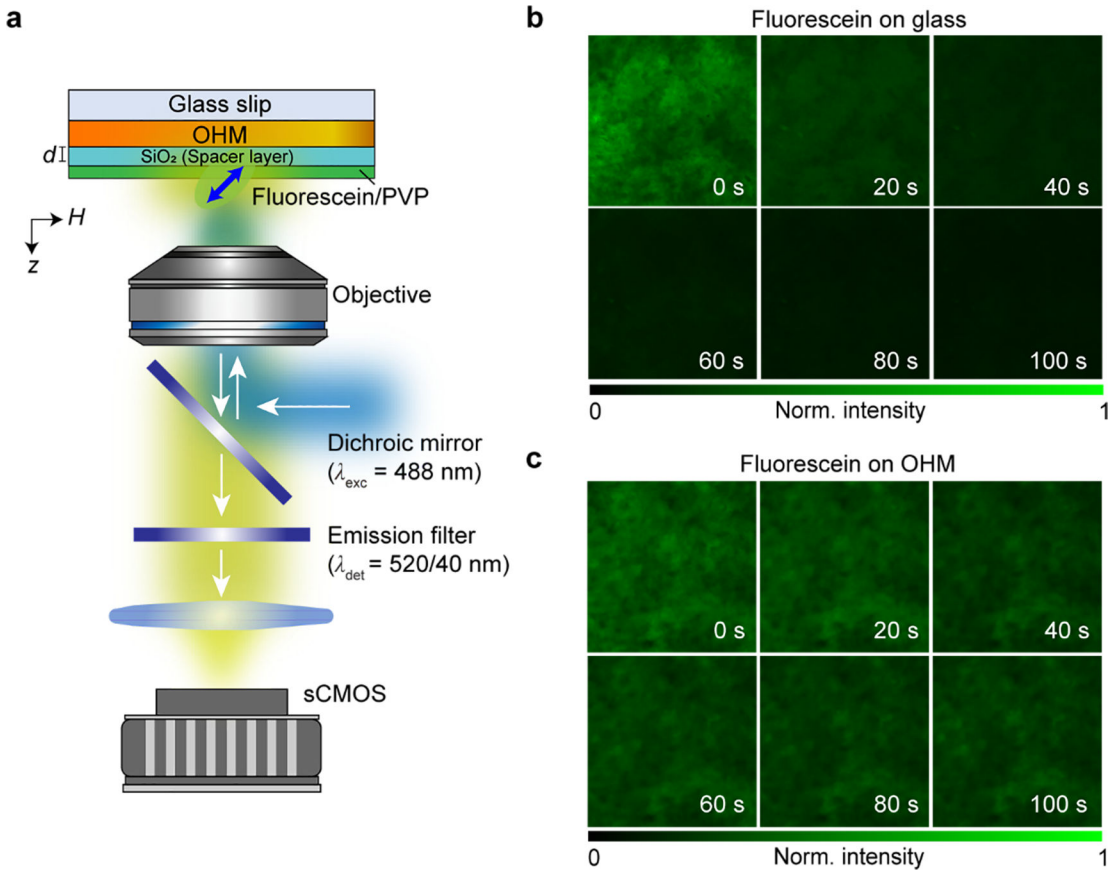

Figure 2.

Experimental set-up and photobleaching response of fluorophores on various substrates. (**a**) Experimental set-up. The normalized emission intensity of fluorophores was monitored over time (at 0, 20, 40, 60, 80, and 100 seconds during the continuous excitation laser exposure on the fluorophore layer). The emission intensity of fluorescein (**b**) on a glass coverslip (control sample) and (**c**) on the OHM film.

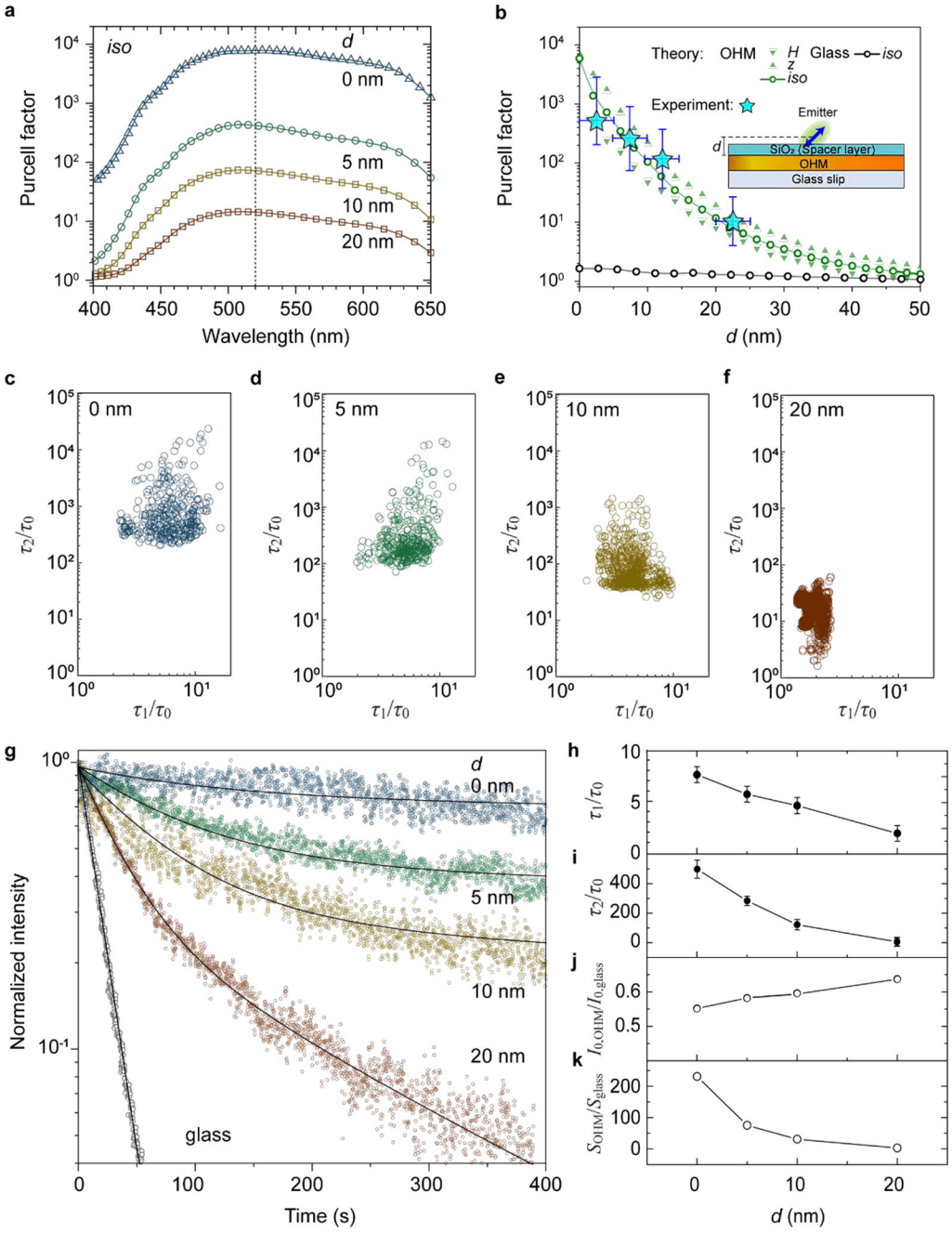

Figure 3.

PF and enhanced photostability for fluorescein on an OHM. (**a**) Calculated *PF* spectra for an isotropic dipole source located at a height of *d* above the OHM substrate. (**b**) Experimental and calculated *PF* for dipole sources (dipole direction: Parallel is given as *H*, perpendicular is given as *z*, and averaged is given as *iso* with respect to substrates) located above the OHM (blue curve) and the glass (black curve) substrates at wavelength λ = 520 nm. (**c**–**f**) Experimentally measured photobleaching suppression rates (τ_1/τ_0 and τ_2/τ_0) of fluorophores located above the OHM surface for d = 0 nm (c), d = 5 nm (d), d = 10 nm (e), and d = 20 nm (f), respectively. (**g**) Normalized emission intensities as a

function of detection time, generated from a 50×50-pixel average corresponding to an area of 8.125×8.125 μm^2. (**h**) Distance dependence of τ_1/τ_0. (**i**) Distance dependence of τ_2/τ_0, where τ_0 corresponds to the photobleaching lifetime of fluorophores on glass. (**j**) Distance dependence of the initial emission intensity $I_{0,\mathrm{OHM}}/I_{0,\mathrm{glass}}$ at $t = 0$, where $I_{0,\mathrm{glass}}$ corresponds to initial emission intensity measured on glass. (**k**) Distance dependence of the integrated emission intensity $S_{\mathrm{OHM}}/S_{\mathrm{glass}} = \sum I_{t,\mathrm{OHM}}/I_{t,\mathrm{glass}}$, where S_{glass} corresponds to integrated emission intensity measured on glass.

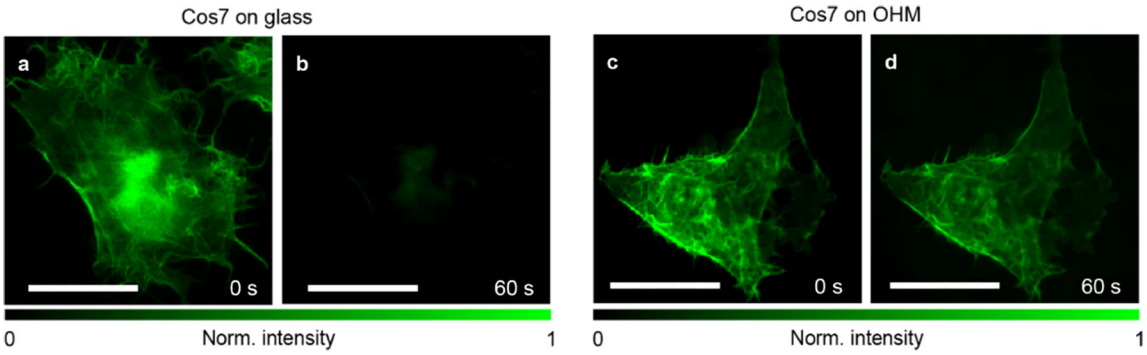

Figure 4.

Photostability enhancement. Fluorophores are much more photostable on OHMs than on glass. Lifeact-Venus tagged Cos-7 cell images are shown after 0 and 60 seconds of 488-nm excitation laser (approximately 61 W/cm^2) exposure. On the glass substrate (**a**,**b**), fluorophores are photobleached almost immediately; highly photostable fluorophores, however, are observed on the OHM substrate (**c**,**d**). The scale bar is 20 μm.

Table 1.

Comparative photobleaching response of fluorescein dye on glass and OHM substrates

Samples	*d* (nm)	Photobleaching lifetime		Photobleaching suppression rate		Initial intensity	Total intensity
Glass	0	τ_0 (s) 15.6		τ_0/τ_0 1		$I_{0,glass}/I_{0,glass}$ 1	S_{glass}/S_{glass} 1
OHM		τ_1 (s)	τ_2 (s)	τ_1/τ_0	τ_2/τ_0	$I_{0,OHM}/I_{0,glass}$	S_{OHM}/S_{glass}
	0	119.8	7897.5	7.7	506.3	0.552	231.3
	5	90.1	4547.5	5.8	291.5	0.582	75.3
	10	72.6	2005.6	4.7	128.6	0.596	30.7
	20	31.3	181.7	2.0	11.6	0.637	2.92